发 光 学 报
CHINESE JOURNAL OF LUMINESCENCE

文章编号：1000-7032(XXXX)XX-0001-19

钙钛矿基宽谱带光电探测器

卢孟涵[1]，宋宏伟[2*]，陈　聪[1*]
（1.河北工业大学 材料科学与工程学院，天津　300401；
2.吉林大学 电子科学与工程学院 集成光电子学国家重点联合实验室，吉林 长春　130012）

摘要：钙钛矿材料凭借可调带隙、高光吸收系数和低激子结合能等优势，在半导体光伏和光电探测领域大放异彩。普适性的铅基钙钛矿吸收范围通常集中在UV到Vis区域，而窄带隙的纯锡基或者锡铅混合钙钛矿其吸收光谱仍局限于~1060 nm以内的近红外范围，受限于未来复杂场景的应用及探测成像。通过将钙钛矿与窄带隙半导体结合构建“钙钛矿/半导体”复合异质结可以进一步扩展光谱范围并提高吸收效率。本综述总结了钙钛矿基宽谱带光电探测器在探测性能优化、单体材料优异性能、复合材料优选工程等方面的进展，并探讨了宽谱探测器在光谱响应、像素集成、柔性器件开发和稳定性等方面的进展和应用前景。本综述将有助于推动钙钛矿基宽谱带光电探测研究及其未来成像应用。

关　键　词：钙钛矿；红外光电探测器；宽谱带光电探测器；量子点；异质结
中图分类号：O649.4　　　**文献标识码**：A　　　**DOI**：10.37188/CJL.20240031

Perovskite Based Broadband Photodetector

LU Menghan[1], SONG Hongwei[2*], CHEN Cong[1*]
(1. *School of Material Science and Engineering*, *Hebei University of Technology*, *Tianjin* 300401, *China*;
2. *State Key Laboratory of Integrated Optoelectronics*, *College of Electronic Science and Engineering*, *Jilin University*, *Changchun* 130012, *China*)
* *Corresponding Authors*, *E-mail*: *chencong@hebut.edu.cn*, *songhw@jlu.edu.cn*

Abstract: Perovskite materials, with their adjustable bandgaps, high light absorption coefficients, and low exciton binding energies, have shone brightly in the fields of semiconductor photovoltaics and photoelectric detection. The absorption range of universal lead-based perovskites is usually concentrated in the UV to Vis region, while the absorption spectra of narrow-bandgap pure tin-based or tin-lead mixed perovskites are still limited to the NIR range within ~1060 nm, constrained by the application and detection imaging in future complex scenarios. Combining perovskites with narrow-bandgap semiconductors to construct "perovskite/semiconductor" composite heterostructures can further expand the spectral range and enhance absorption efficiency. This review summarizes the progress in optimizing detection performance, the exceptional properties of monomaterials, and the preferred engineering of composite materials for perovskite-based broadband photodetectors. It also discusses the advancements and application prospects of broadband detectors in terms of spectral response, pixel integration, development of flexible devices, and stability. This review aims to promote research in perovskite-based wide-band photodetection and its future imaging applications.

Key words: Perovskite; Infrared Photodetectors; Broadband Photodetectors; Quantum Dots; Heterojunctions.

收稿日期：XXXX-XX-XX；**修订日期**：XXXX-XX-XX
基金项目：国家自然科学基金(62004058，U21A2076)
Supported by National Natural Science Foundation of China(62004058，U21A2076)

1 引 言

根据光电探测器的不同工作波段，分为紫外（UV）、可见光（Vis）和红外光（IR）（图 1）[1]。其中 UV 光电探测器常使用氮化镓等宽禁带半导体，应用于环境监测等领域。Vis 光电探测器多采用硅（Si）基材料，来支撑现阶段电子产品数码成像产业，在商业应用中 Si 基探测器最为常见，但其 1.1 eV 带隙限制了光谱带宽，因此只能识别光强信息，无法独立区分偏振、波长和入射角度等信息，该缺点大大限制了其应用范围。IR 光电探测器采用铟镓砷、碲化镉汞等材料，广泛应用于夜视、光通讯和国防侦查等领域，但其成本高昂且需低温制冷。近年来，随着对同一场景进行多波段（UV、Vis、IR）光电探测的需求增加，促进多光谱联用和交叉探测技术的发展。然而，目前的光电探测技术通常只能对单一波长进行有效响应，实现宽光谱响应仍然是一个挑战[2, 3]。

钙钛矿材料近年来在光电领域备受瞩目[4, 5]。相较于传统半导体，钙钛矿具有窄带光探测、偏振光探测和 X-Ray 探测等优异特性[6-9]本文通过对钙钛矿组分工程、复合层设计、器件构筑、调控器件性能方法、工作机制等方面进行分析，对钙钛矿基宽谱带光电探测器进行总结概述。首先，对单体铅（Pb）基和锡（Sn）基钙钛矿宽谱光电探测器的设计以及器件构筑方法进行总结。其次，综述了钙钛矿/复合材料（有机、GaAs、Si、量子点（QDs）等）的宽谱带光电探测器的类型、工作机制和响应特性。最后，讨论近年来出现的相关实际应用，以及对钙钛矿基宽谱带光电探测器的未来展望。

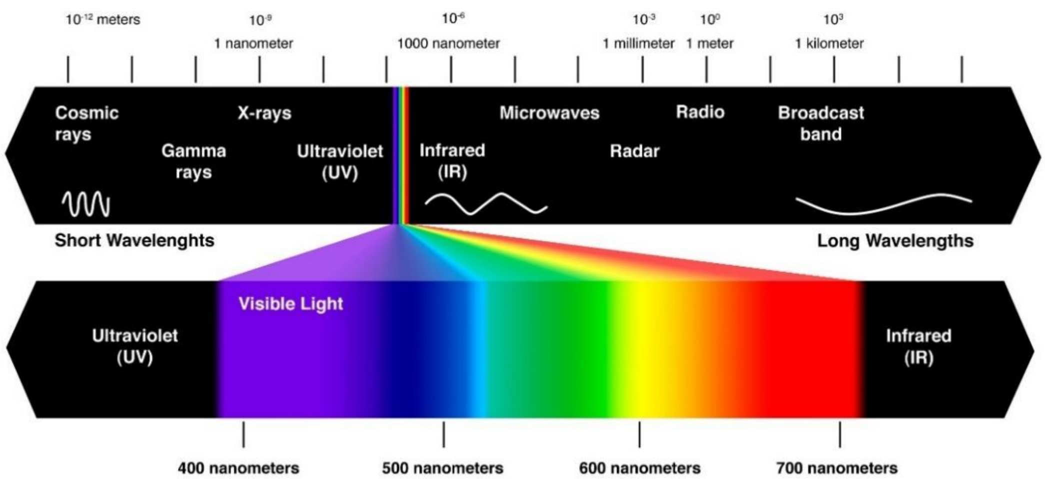

图 1 电磁波谱[10]

Fig. 1 electromagnetic spectrum[10]

2 单体钙钛矿宽谱带光电探测器

目前，Pb 基钙钛矿最低带隙约为 1.45 eV（$FAPbI_3$），只能有效覆盖 UV-Vis 波段，而在 NIR 区域的响应较弱。通过 Sn 部分或完全替代 Pb 可实现具有 NIR 吸收的窄带隙卤化物钙钛矿。然而，含 Sn 钙钛矿存在严重的 Sn^{2+} 氧化为 Sn^{4+} 问题[11]（图 2）。

3.1 Pb 基钙钛矿宽谱带光电探测器

Pb 基钙钛矿在 IR 的吸收系数（10^{-5} cm）比 GaAs 还要高一个数量级[13]，兼具缺陷容忍度高的优势。受半导体带隙的限制，纯 Pb 基钙钛矿只可以实现最宽到约 850 nm 的光电探测响应[14-18]。Fang 等[19]将 $MAPbI_3$ 晶体（禁带宽度即 Eg≈1.55 eV）切成薄片，并在其表面沉积 Au 电极作为光电探测器（图 3a），具有半高宽小于 20 nm 的窄光谱响应。Paul 等[14]通过改变半导体中卤素的混合比例或在薄膜中添加有机分子来形成复合结构，并使用升温结晶法生长了毫米大小的 $MAPbBr_3$ 和 $MAPbI_3$ 单晶，该探测器能够实现对约 1060 nm 波长响应。

与单晶相比，多晶 Pb 基钙钛矿能够探测更宽波段。Xie 等[20]通过在柔性 ITO 衬底上沉积 $MAPbI_3$ 薄膜，在 3 V 偏压下提高了在 365 nm 和 780 nm 处的光响应率和外量子效率。Xiao 等[21]通过蒸气辅助溶液法制备了平均晶粒尺寸为 1.5 μm 的 $MAPbCl_3$，基于该薄膜制备的光电探测器对 UV 表

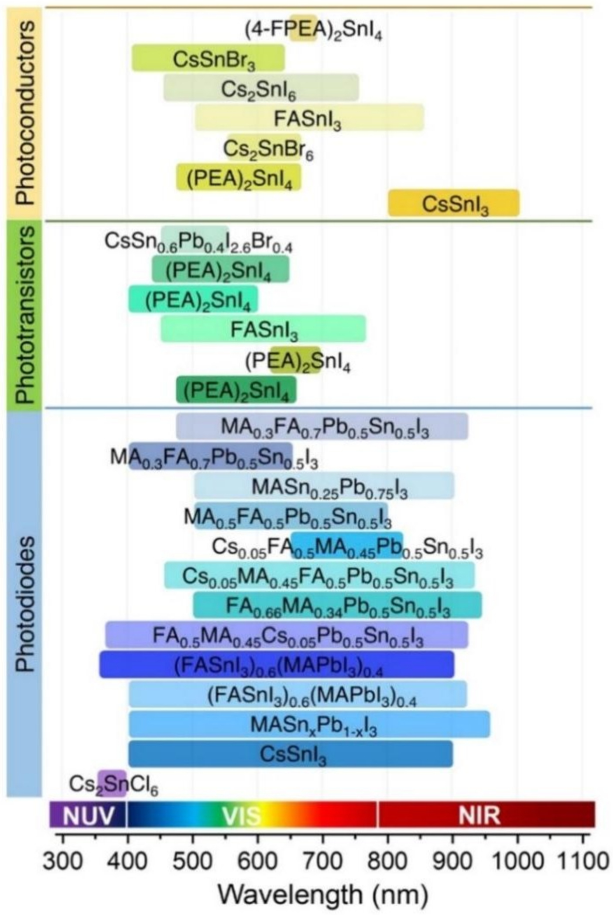

图2　已报道用于不同类型的光电探测器的不同Sn基和Sn-Pb基钙钛矿[12]

Fig 2　Spectrum range of different Sn and Sn-Pb perovskites photodetectors, which have been reported for different types of photodetectors[12]

现出297 mA/W的响应(图3b)。然而,由于Pb基钙钛矿的宽带隙问题,寻找合适的材料代替Pb以获得低毒、窄带隙的钙钛矿是研究人员的目标[22]。

3.2　Sn基钙钛矿宽谱带光电探测器

理论和实验结果证明Sn基钙钛矿具有与Pb基钙钛矿相似的性质,且已经证明了其在各种器件应用中的可行性,特别是在扩展到900 nm范围以外的NIR波段。Sn基钙钛矿太阳能电池的PCE超过14.2%[23-26]。典型Sn基钙钛矿有$FASnI_3$、$CsSnI_3$、$MA_{0.5}FA_{0.5}SnI_3$等,其带隙约为1.2-1.4 eV,室温下激子结合能低于25 meV,载流子扩散长度超过500 nm[27]。

提高电荷收集效率、抑制Sn的氧化是Sn基钙钛矿的研究重点[28, 29]。如图3c所示,通过引入抗氧化化合物作为添加剂来控制Sn基钙钛矿的快速生长和抑制Sn氧化。Liu等[30]通过氢醌磺酸和$SnCl_2$添加剂,得到$FASnI_3$基的高灵敏度光电探测器。氢醌磺酸使$SnCl_2$在$FASnI_3$中实现均匀分布,并且具有从UV到NIR的宽带响应,光电导体[31]和光电晶体管[32]的最大响应率分别为10^5 A/W和$2.6×10^6$ A/W。Yan等[33]在$FASnI_3$生长过程中加入羟基磺酸和$SnCl_2$作为添加剂,制备Au/$FASnI_3$/Au器件在300-1000 nm的宽谱带具有超过10^5 A/W的高响应性。此外,反溶剂法生长$CsSnI_3$薄膜也受到广泛研究,控制相纯度和Sn空位的形成是关键[34]。该课题组在$CsSnI_3$前驱体中加入含有还原剂抗坏血酸的添加剂,采用反溶剂法制备$CsSnI_3$薄膜(图3d)[35],在350-1000 nm得到0.35 /1.6 ms的快响应时间,0.257 A/W的高响应度。此外,Shao等[36]通过热注射法合成Cs_2SnI_6,并通过原子层沉积ZnO增强载流子分离,从而将探测率提高到10^{11} Jones。2022年,Krishnaiah等[37]引入HI优化Cs_2SnI_6前驱体获得6个月以上的长期运行稳定性,在455-740 nm宽范围内探测器具有10 A/W响应度,$7.9×10^{10}$ Jones探测率。

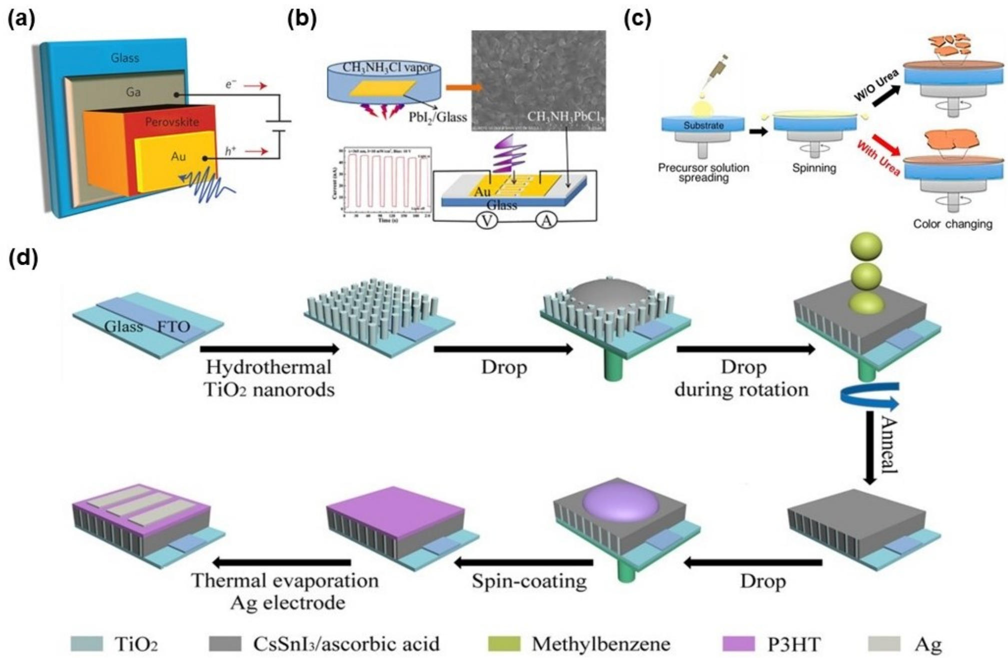

图3 (a)钙钛矿表面沉积Au电极阵列的器件结构示意图[19];(b)蒸气辅助溶液法制备$MAPbCl_3$基器件工作图[21];(c)薄钙钛矿膜的旋涂过程以及添加剂对膜形态[38];(d)$MASnI_3$ NW阵列的光电探测器结构图[35]

Fig. 3 (a) Schematic device structure of perovskite surface-deposited Au electrode array[19]; (b) Schematic of the operation of $MAPbCl_3$-based devices prepared by vapor-assisted solution process[21]; (c) Spin coating process of a thin perovskite film[38]; (d) Schematic illustration of the photodetector structure with $MASnI_3$ nanowire arrays[35]

3.3 Sn-Pb钙钛矿宽谱带光电探测器

Sn-Pb混合体系钙钛矿的带隙可低至1.17 eV,NIR吸收波长可达1060 nm[39,40]。此外,与纯Sn基钙钛矿相比,Sn-Pb钙钛矿具有更高的稳定性[41],更低的暗电流密度、更高的响应率和长载流子寿命[42]。随着Sn含量的增加,Sn-Pb混合钙钛矿材料在光电物理性质方面的一个重要特征是:从小极化子到大极化子的转变,表明缺陷减少[43]。Zhao等[44]发现随着钙钛矿厚度的增加,器件对长波长的光(>650 nm)具有增强的干涉效应,从而收获更多的入射IR光子。如图4a所示,采用1.25 eV的窄带隙$(FASnI_3)_{0.6}(MAPbI_3)_{0.4}$,增加层厚度可以提高NIR区域的EQE值并降低暗电流。由于Sn氧化会形成Sn空位,Jen等[45]引入抗坏血酸来抑制Sn^{2+}的氧化,从而得到350-1000 nm的宽带光电探测器(图4b)。抗坏血酸延缓Sn空位的形成,促进薄膜的生长。为了稳定Sn-Pb混合钙钛矿,Shen等[46]采用双面钝化策略—在$Cs_{0.05}MA_{0.45}FA_{0.5}Pb_{0.5}Sn_{0.5}I_3$层的上下两侧同时引入PEAI钝化层(图4c-d)。与单面钝化相比,优化后的Sn-Pb混合钙钛矿光电探测器在-0.1 V下具有300-1050 nm的宽带响应,1.25×10^{-3} mA/cm^{2}的低暗电流密度,35 ns的响应速度。

Sn-Pb窄带隙混合钙钛矿单晶作为高效、低成本NIR光电探测器的材料非常有前景。然而,由于Pb基和Sn基钙钛矿的结晶速度存在差异,Sn-Pb混合钙钛矿在结晶过程中容易发生相分离,导致材料的光学和电子性能下降。Li等[47]通过电负性平衡的策略制备具有优异结晶度和定向生长的Sn-Pb混合钙钛矿—$Cs_{0.05}MA_{0.45}FA_{0.5}Sn_{0.5}Pb_{0.5}I_3$,基于该材料的探测器表现出350-1000 nm的宽带响应和高性能NIR检测能力,同时其响应时间为2 μs,响应率为0.29 A/W。同时,基于该材料制备柔性Sn-Pb钙钛矿器件在空气中未封装条件下经历3000次弯曲循环后仍然表现出快速响应。Jie等[48]通过一种低温空间限制技术,可同时降低纯Sn和Pb钙钛矿的结晶速度,得到$(FASnI_3)_{0.1}(MAPbI_3)_{0.9}$单晶,具有高达163.5 dB宽线性动态范围,在750-860 nm的NIR区域具有22.78 μs的快速响应速度。Xu等和Wang等[44]分别引入$MA_{0.5}FA_{0.5}Pb_{0.5}Sn_{0.5}I_3$和$MA_{0.4}FA_{0.6}Pb_{0.4}Sn_{0.6}I_3$,减小带隙促进NIR光子的吸收。优化后的光电探测器在1000 nm NIR区域表现出良好的光响应。

2022年,Chang等[49]使用UiO-66-NH_2作为添加剂,得到器件在650-810 nm的NIR区域具有高达0.35 A/W的响应度,以及1.54×10^{13} Jones的探

测率。Kim 等[50]通过将手性等离子体金纳米颗粒掺杂到 Sn-Pb 钙钛矿中，探测器无需外部电源输入即可工作，在 470-910 nm 实现 0.6 A/W 的高响应度，以及 1.5×10^{12} Jones 的高探测率。Liu 等[51]采用硫氰酸锡在 Sn-Pb 钙钛矿中形成双面分布，获得 910 nm NIR 区域响应的自供电 Sn-Pb 钙钛矿光电探测器，响应度和探测率分别达到了 0.57 A/W 和 8.48×10^{12} Jones。2024 年，Li 等[47]通过混合 Sn-Pb 钙钛矿和电负性平衡的协同作用，获得具有优异晶体性和选择性生长取向的窄带隙高稳定性 $Cs_{0.05}MA_{0.45}FA_{0.5}Sn_{0.5}Pb_{0.5}I_3$ 薄膜，探测器具有 350-1000 nm 的宽带响应能力，2 μs 的快速响应和 0.29 A/W 的高响应度。

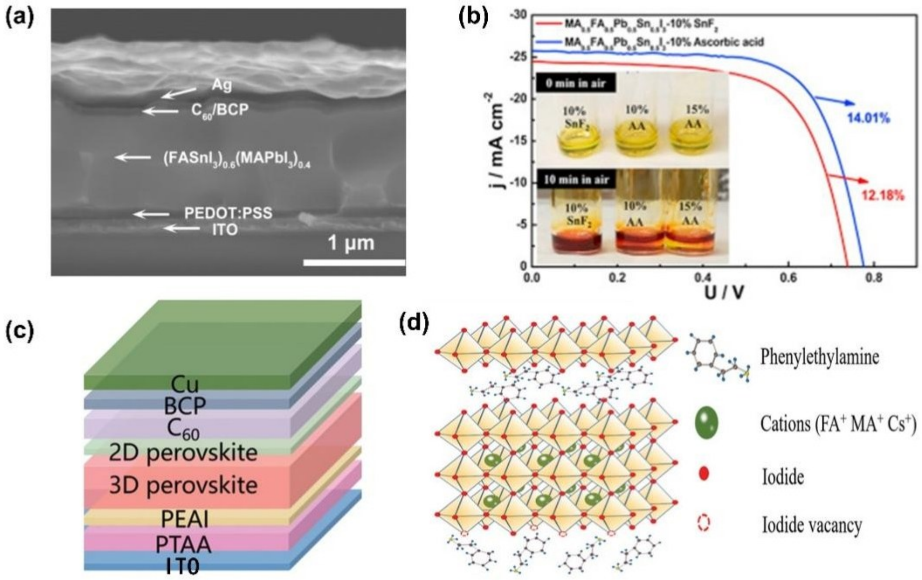

图 4(a) Sn-Pb 混合探测器件的截面 SEM 图像[44]；(b)掺杂抗坏血酸的器件的 J-V 曲线图[45]；(c)基于 3D-perovskite/2D-perovskite 光电探测器结构；(d) PEAI 钝化碘空位和 2D 低维钙钛矿示意图[46]

Fig. 4 (a) Cross-sectional SEM image of a Sn-Pb mixed detector device[44]; (b) Current-voltage J-V curve diagram of a device doped with ascorbic acid[45]; (c) Schematic illustration of a photodetector based on 3D-perovskite/2D-perovskite; (d) Schematic of PEAI passivating iodine vacancies and 2D low-dimensional perovskite[46]

4 钙钛矿/复合材料宽谱带光电探测器

尽管纯 Sn 或者 Sn-Pb 混合钙钛矿有更广泛的光子吸收范围，但二者的吸收光谱仍局限于 1060 nm 的 NIR 和 Vis 范围内。因此，通过将其它半导体组分引入钙钛矿构建异质结，可为设计和拓宽钙钛矿光电探测器 IR 区域的响应性能带来更多的可能性[52]。钙钛矿结构与有机/无机材料结合构建同质结、平面异质结或体异质结，不仅丰富器件结构的多样性还降低暗电流，从而显著提高分辨率和灵敏度[53-56]。2019 年，Fu 等[57]构建钙钛矿/MoS_2 异质结显著提升光电探测器的性能，探测率和光响应率分别提高了 2 和 6 个数量级，这表明钙钛矿和 MoS_2 界面处的电荷分离很容易(图 5a)。

4.1 基于钙钛矿/有机材料宽谱带光电探测器

将钙钛矿和有机半导体结合，通过分子设计可以拓宽光谱的响应范围，能将范围从 Vis 扩展到 IR 光谱范围，因此制备高灵敏、快响应的钙钛矿有机异质结光电探测器近年来受到越来越多的关注。图 6 根据其光学吸收范围总结了应用于光电探测器的有机半导体材料[58]。目前，钙钛矿/有机复合探测器的快响应时间对于开发超快响应、高性能宽带光电探测器具有重要意义。

得益于窄带隙共轭聚合物在 Vis-NIR 的光吸收和有利的能带结构，Li 等[59]通过压印方法制备有序的 $CsPbBr_3$ NW 阵列与 PDPP3T 复合，获得在 UV-NIR 区域敏感的自供电光电探测器(图 5b)，该器件在 300-950 nm 宽光谱范围内得到高达 0.25 A/W 的响应度，1.2×10^{13} Jones 的探测率以及 111/306 μs 的响应速度。同样，Shi 等[60]在叉指金电极的 PET 柔性基板上依次旋涂 $MAPbI_3$ 和 PDPP3T 溶液制备光电探测器，如图 5c 所示，$MAPbI_3$/PDPP3T 异质结光电探测器在 1 V 下具有

UV-NIR的宽带光电检测特性。PDPP3T涂层不仅拓宽其NIR区域检测范围，还提高其响应度和探测率。此外，PDPP3T涂层还用作$MAPbI_3$膜的保护层，提高探测器环境稳定性。Shen等[61]将$MAPbI_3$与F8IC:PTB7-Th复合制备在NIR区域具有高检测性能的宽带光电探测器，将响应光谱扩展到1000 nm。近年来，一些共轭聚合物半导体（如PEDOT:PSS、PDVT-10和PDPP-TT）也被用于与卤化物钙钛矿复合构建异质结光电探测器。如图5d所示，Yan等[62]报道一种PEDOT:PSS/$MAPbI_{3-x}Cl_x$基光电探测器，在UV-NIR的宽光谱区域中表现出约109 A/W的超高响应度和10^{14} Jones的探测率。此外，这种高性能异质结也可以复合在聚酰亚胺衬底上，制备的柔性光电探测器具有良好的机械柔性和弯曲耐久性。Shen等[63]制备$MAPbI_3$和PDPPTDTPT复合光电探测器，其探测波长扩展到950 nm，响应时间达到5 ns。为提高NIR的EQE，Wu等[64]通过在$MAPbI_3$上涂覆PTB7-Th:IEICO-4F，获得在340-940 nm区域EQE响应达到70%的宽带光电探测器（图5e），该异质结有效促进钙钛矿和有机层之间光生电荷的提取和传输，具有优化结构的集成光电探测器在Vis-IR区域的EQE大多超过70%。

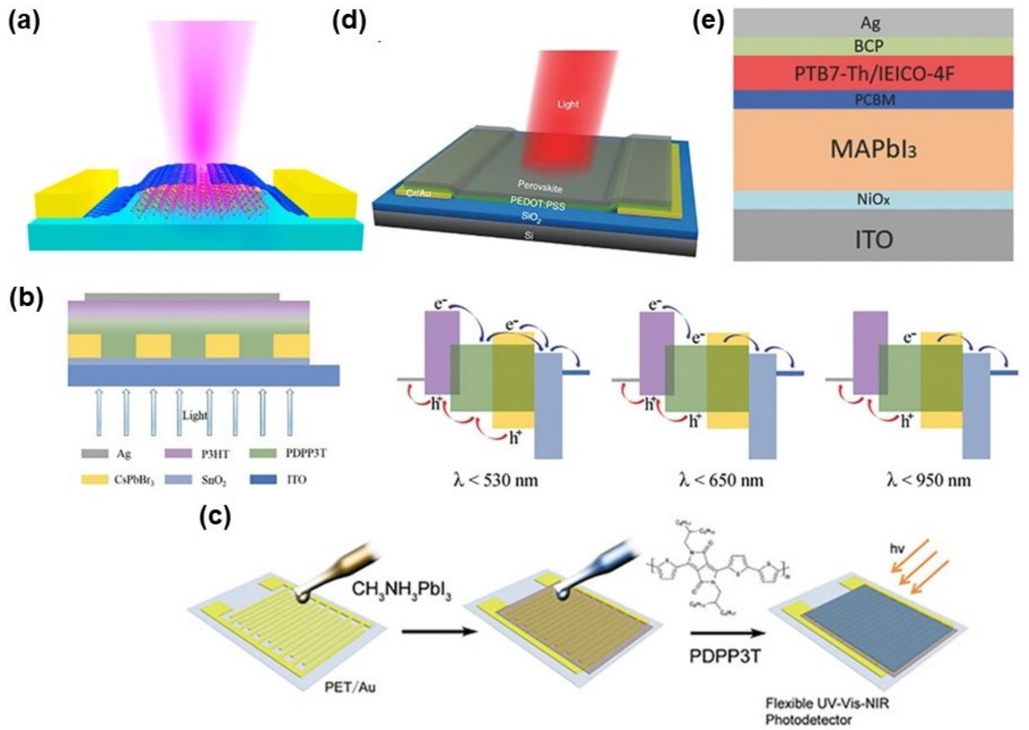

图5（a）钙钛矿/MoS_2界面处的电荷分离示意图[57]；（b）基于$CsPbBr_3$ NW/PDPP3T异质结光电探测器及在不同光波长照射下的载流子传输过程的示意图[59]；（c）基于$MAPbI_3$/PDPP3T的柔性光电探测器制备的示意图[60]；（d）基于$MAPbI_{3-x}Cl_x$/PEDOT:PSS异质结的光电探测器的示意图[62]；（e）ITO/NiO_x/$MAPbI_3$/PCBM/PTB7-Th:IEICO-4F/BCP/Ag光电探测器结构[64]

Fig 5 (a) Schematic illustration of charge separation at the perovskite/MoS_2 interface[57]; (b) Schematic illustration of a $CsPbBr_3$ NW/PDPP3T heterojunction photodetector and the carrier transport process under illumination of different wavelengths[59]; (c) Schematic illustration of the fabrication of a flexible photodetector based on $MAPbI_3$/PDPP3T[60]; (d) Schematic illustration of a photodetector based on the $MAPbI_{3-x}Cl_x$/PEDOT:PSS heterojunction[62]; (e) Photodetector structure of ITO/NiO_x/$MAPbI_3$/PC61BM/PTB7-Th:IEICO-4F/BCP/Ag[64]

为了实现UV-NIR范围的高性能宽带探测器，研究人员使用在NIR区域具有良好光电响应的有机光电材料Y6分子[65]（图7a）。其设计改善分子间相互作用、调节能级以及优化溶解性和形貌。特别是，Y6分子氟化策略增强分子间或分子内的氢键或卤素键，改善分子的填充和形貌。Zhao等[66]引入Y6与PM6一起形成异质结，从而扩宽钙钛矿探测器的响应光谱。通过钙钛矿和有机层的协同效应，可以实现高性能自供电钙钛矿/有机宽带光电探测器，实现300-1000 nm的宽谱带

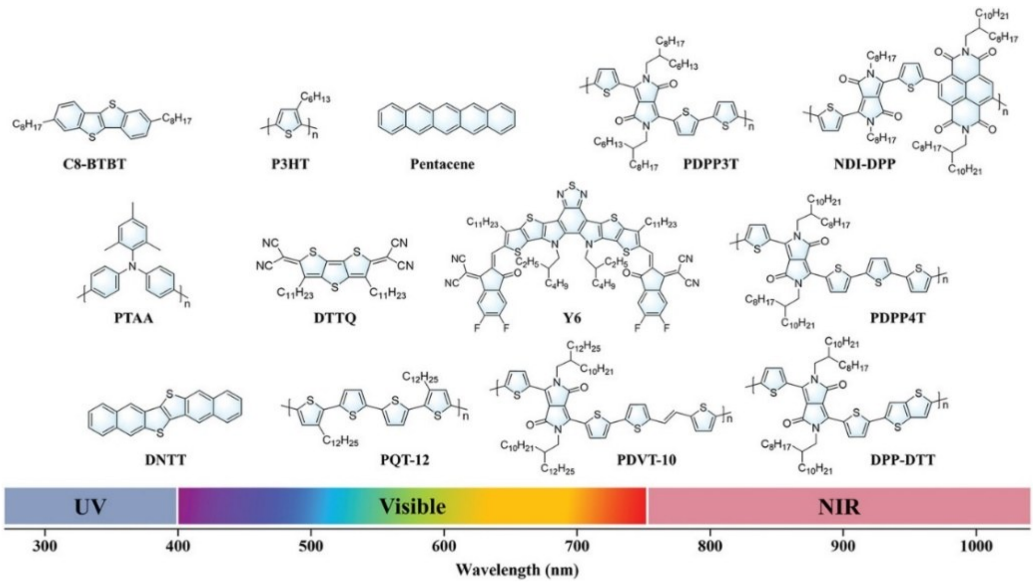

图6 有机半导体材料在光电探测器中的应用概述，分子结构式是根据材料的光学吸收范围排列的[58]

Fig. 6 Summary of the organic semiconductor materials applied in photodetector, the molecular structure formulas are ordered according to the optical absorption range of the materials[58]

探测范围(图7b)，具有高达80%的EQE。同样是利用Y6分子，Gao等[67]成功制备$Cs_{0.15}FA_{0.85}PbI_3$/$PC_{61}BM$:D_{18}:Y6异质结光电探测器(图7c)，具有高低能光子收集能力，可以扩展至931 nm。在Y6和$MAPbI_3$混合体系钙钛矿光电探测器的基础上，Zhang等[68]进一步在钙钛矿层和聚合物层之间引入PFN界面层，有助于选择性地传递载流子，过滤信号光谱中的短波长光。基于Y6的混合探测器 (ITO/PEDOT: PSS/$MAPbI_3$/PFN/PM6: Y6/C_{60}/BCP/Ag)在无偏压下的最高EQE达到83.7%，高达1.52×10^{13} Jones的探测率，NIR响应度为0.577 A/W，快响应时间为1.73/0.97 μs，光谱范围在770-900 nm之间。不只是利用钙钛矿薄膜，Chen等[69]将$CsPbBr_3$ QDs与PDVT-10和Y6分子结合获得宽谱带光电探测器，双层PQD/PDVT-10平面异质结的光电探测器在450 nm获得1.64×10^4 A/W的响应度，3.17×10^{12} Jones的探测率，以及5.33×10^6的光敏度。其光探测性能归因于PQD/PDVT-10平面异质结中电荷的有效分离和传输。此外，三层PDVT-10/PQD/Y6平面异质结构建自供电光电探测器，得到UV到NIR的光响应，响应度接近10^{-1} A/W，探测率超过10^6 Jones。这些结果表明溶液加工钙钛矿材料与Y6等有机分子构筑平面异质结能够实现宽光谱响应。

除了共轭聚合物半导体外，近年来还研究了一些有机小分子半导体，如C8-BTBT[70,71]。如图7d所示，Yang等[72]使用溶液处理的C8-BTBT/$MAPbI_3$复合制备高性能光电探测器，具有UV-Vis区域的宽光谱响应。得益于C8-BTBT膜的高空穴迁移率和界面处的有效空穴转移，该探测器具有高达24.8 A/W的响应度、2.4×10^4的高I_{light}/I_{dark}和约4 ms的响应速度。此外，C8-BTBT涂层可以作为$MAPbI_3$薄膜的保护层抵抗湿气侵蚀，使设备在40%-50%的相对湿度下储存20天后保持90%的性能。

4.2 钙钛矿/半导体晶体宽谱带光电探测器

4.2.1 钙钛矿/GaAs宽谱光电探测器

无机半导体具有化学稳定性、低成本、适当能级和高载流子迁移率等特性，有助于电荷传输、提高钙钛矿稳定性[90]。GaAs具有1.42 eV直接带隙和高电子迁移率，适用于制备各种光电器件[91-93]，如太阳能电池[94,95]、光电探测器[96]、p-n二极管[97]和场效应晶体管[98]。Zhao等[99]制备了钙钛矿/GaAs光电探测器，该器件在530 nm照射下具有高达0.3 A/W的响应度、2.24×10^{10} Jones的探测率以及0.6/0.56 ms的上升/下降时间。2023年，Hou等[100]制备一维无机GaAs NW和二维钙钛矿材料的复合光电探测器(如图8a)，在UV-Vis的响应率和探测率显著提高，分别达到75 A/W和1.49×10^{11} Jones，响应时间缩短了3个数量级，从785降至0.5 ms，同时暗电流进一步降低至237 mA。图8b、c为该混合结构的能带图和吸收光谱，优异的

表1 基于有机材料/钙钛矿光电探测器的性能

Table 1 Performance of photodetector based on organic / perovskite

复合类型	器件结构	λ(nm)	R(A/W)	D(Jones)	I_{light}/I_{dark}	(τ_{rise}/τ_{decay})	LDR(dB)	Ref
钙钛矿/有机材料	PEDOT:PSS/$MAPbI_3$/PCBM	300-800	-	$>10^{12}$	-	1.7/1.1 μs	≈170	[73]
	PEDOT:PSS/$MAPbI_3$/PCBM:PMMA	300-800	-	1.1×10^{13}	-	3.0/2.2 μs	112	[74]
	P3HT-COOH/$MAPbI_3$/PCBM	330-800	0.497	3.03×10^{13}	-	95 μs	200	[75]
	PEDOT:PSS/$FAPbI_3$/PCBM	330-800	0.3	5.0×10^{11}	2.72×10^4	1.7/21.2 μs	136	[76]
	$CsPbBr_3$/PDPP3T	300-950	0.25	1.2×10^{13}	-	111/306 μs	-	[59]
	PTAA/MAPbI3/F8IC:PTB7-Th	300-1000	-	2.3×10^{11}	-	5.6 ns	191	[61]
	$MAPbI_3$/PCBM/PTB7-Th:IEICO-4F	340-940	0.518	$>10^{10}$	-	0.50/0.51 ms	-	[64]
	PEDOT:PSS/$(FASnI_3)_{0.6}(MAPbI_3)_{0.4}/C_{60}$	350-950	>0.4	$>10^{12}$	-	6.9/9.1 μs	167	[44]
	PEDOT:PSS/$MAPbI_3$/PCBM	300-800	0.321	-	-	4.0/3.3 μs	84	[77]
	PEDOT:PSS/Sn-rich binary perovskite/PCBM	360-985	0.2	$>10^{11}$	-	0.09/2.27 μs	100	[78]
	PTAA/$MAPbBr_3$/COi8DFIC	300-960	0.16	1.34×10^{12}	-	54/567 μs	-	[79]
	PTAA/$MAPbI_3$ NWs/DPP-CNTVT	400-940	0.5	$>10^{13}$	-	0.27/0.21 μs	265	[80]
	PTAA/$FA_{0.5}MA_{0.45}Cs_{0.05}Pb_{0.5}Sn_{0.5}I_3$/TBA-Azo	300-1050	0.45	2.21×10^{11}	-	42.9 ns	185	[81]
	$MAPbI_3$/C8-BTBT	350-808	24.8	7.7×10^{12}	2.4×10^4	4.0/5.8 ms	-	[72]
	$MAPbI_3$/PDPP3T	365-937	0.026	8.8×10^{10}	-	-	-	[60]
	$MAPbI_3$+C8-BTBT	365-808	8.1	2.17×10^{12}	9.75×10^3	7.1 ms	-	[82]
	DPPDTT/$CsPbI_3$ QDs	350-940	110	2.9×10^{13}	6×10^3	3.2/3.3 s	-	[83]
	PEDOT:PSS/$MAPbI_{3-x}Cl_x$	370-895	2×10^9	1.7×10^{14}	-	4.5/57.5 s	-	[62]
	P3HT/$MAPbI_{3-x}Cl_x$	350-1300	4.3×10^9	-	-	-	-	[84]
	$MAPbI_3$ nanoparticles+C8-BTBT	252-780	1.72×10^4	2.09×10^{12}	-	-	-	[85]
	$FA_{0.85}Cs_{0.15}PbI_3$+1% PCBM/DNTT	250-800	5.96×10^3	7.96×10^{13}	3.9×10^5	2.3/3.3 ms	-	[86]
	$MAPbI_3$/PM6:Y6/C_{60}	300-1000	0.52	2.86×10^{12}	-	803/698 ns	143	[66]
	PEDOT/$MAPbI_3$/PFN/PM6:Y6/C_{60}	700-900	0.577	1.52×10^{13}	-	1.73/0.97 μs	-	[68]
	$CsPbBr_3$/PDVT-10/PQD/Y6	350-850	0.0028	3.17×10^{12}	5.33×10^6	-	-	[69]
钙钛矿/碳材料	PEDOT:PSS/$MAPbI_xBr_{3-x}$:SWCNTs/PCBM	400-1200	65	3.8×10^{12}	9.3×10^5	15 μs	-	[87]
	PEDOT:PSS/$MAPbI_3$:SWCNTs/NDI-DPP:PCBM	532-1064	0.4	6×10^{12}	-	4.32/12.16 μs	90	[88]
钙钛矿/染料材料	PEDOT:PSS/dye-$FA_{0.83}Cs_{0.17}Pb(I_{0.9}Br_{0.1})_3$/PCBM	800-1600	-	2×10^8	-	65/74 μs	-	[39]
钙钛矿/QDs	PTAA/$MAPbI_3$/PbSe QDs	300-2600	0.23	$>10^{11}$	-	4/32 μs	70	[89]

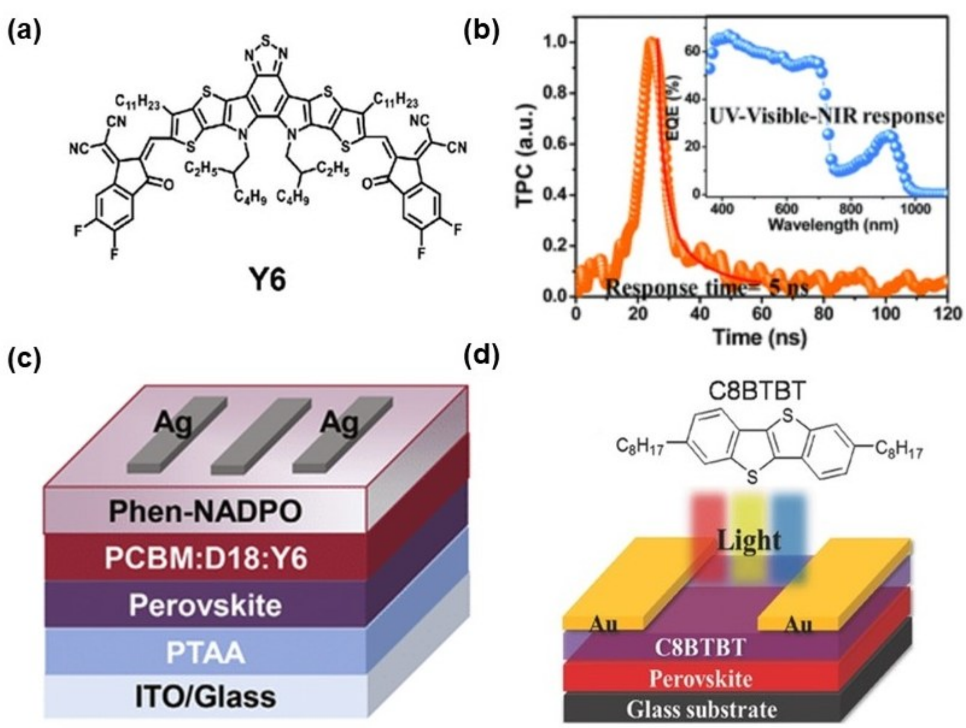

图7 (a)非富勒烯受体Y6分子结构图[65]；(b)钙钛矿/有机混合宽带光电探测器的光谱响应范围[66]；(c) $Cs_{0.15}FA_{0.85}PbI_3$/$PC_{61}BM$：D_{18}：Y6异质结光电探测器结构[67]；(d)$MAPbI_3$/C8BTBT异质结光电探测器结构图，C8BTBT的分子结构图[72]

Fig. 7 (a) Molecular structure diagram of non-fullerene acceptor Y6[65]; (b) Spectral response range of perovskite/organic hybrid broadband photodetector[66]; (c) Structure of $Cs_{0.15}FA_{0.85}PbI_3$/$PC_{61}BM$:D_{18}:Y6 heterojunction photodetector[67]; (d) Schematic illustration of a $MAPbI_3$/C8BTBT heterojunction photodetector structure, with a molecular structure diagram of C8BTBT[72]

光电性能使其成为广泛光电应用的潜在候选材料。

4.2.2 钙钛矿/Si宽谱带光电探测器

Si具有≈1.1 eV的带隙，已广泛与钙钛矿集成用于高灵敏度和宽带光探测。Zhang等[101]制备$MAPbI_3$/Si基的8×8个器件单元光电探测器阵列并应用于图像传感，在黑暗环境中具有明显的整流行为，能够记录970 nm光照产生的"H"图像。此外，单晶钙钛矿光电导器件通常受到响应时间限制(>10 μs)，但是在Si上集成钙钛矿可以实现宽光谱和高速检测。Geng等[102]通过反溶剂蒸气辅助结晶法，直接在Si晶片上集成单晶$MAPbBr_3$，具有405-1064 nm的宽光谱范围，在-1 V偏压下高达5.9×10^{10} Jones的探测率和高达520 ns的超快响应时间。为了拓宽Si NW /钙钛矿复合NIR光电探测器的光谱探测范围，Wu等[103]通过在垂直p型Si NW阵列上涂覆$CsFAPbI_3$，探测器在850 nm照明下得到高达14.86 mA/W响应率和2.04×10^{10} Jones的探测率。Li等[104]在n型Si和钙钛矿层界面插入TiO_2层改善载流子分离并减少复合，使得探测器光谱响应能扩展到1150 nm波长。

4.2.3 钙钛矿/Ge基半导体宽谱带光电探测器

除Si以外，传统半导体材料(如Ge、InGaAs和HgCdTe)在IR波段具有较高的响应探测性能。钙钛矿/Ge异质结能得到高性能宽带光电探测器，2019年，Hu等[105]通过结合无机半导体Ge和$MAPbI_3$，利用蒸汽-溶液工艺在Ge层上形成均匀且无针孔的钙钛矿薄膜，如图9a所示。这种光电探测器相比于单一材料的器件，具有更宽的带宽和更好的性能。该异质结光电探测器中，钙钛矿中光生电子部分转移到Ge中，导致光导增益增强。在680 nm波长处，该器件展现出228 A/W的响应度和1.6×10^{10} Jones的探测率。进一步优化钙钛矿厚度，此器件在1550 nm处具有1.4 A/W的最高响应度，钙钛矿/Ge异质结具有从UV到IR的宽带探测范围。2023年，Yang等[106]制备$CsPb(BrCl)_3$:Yb^{3+}/Ge的金属-半导体-金属结构的宽带光电探测器，探测范围为254-1800 nm。与单一Ge

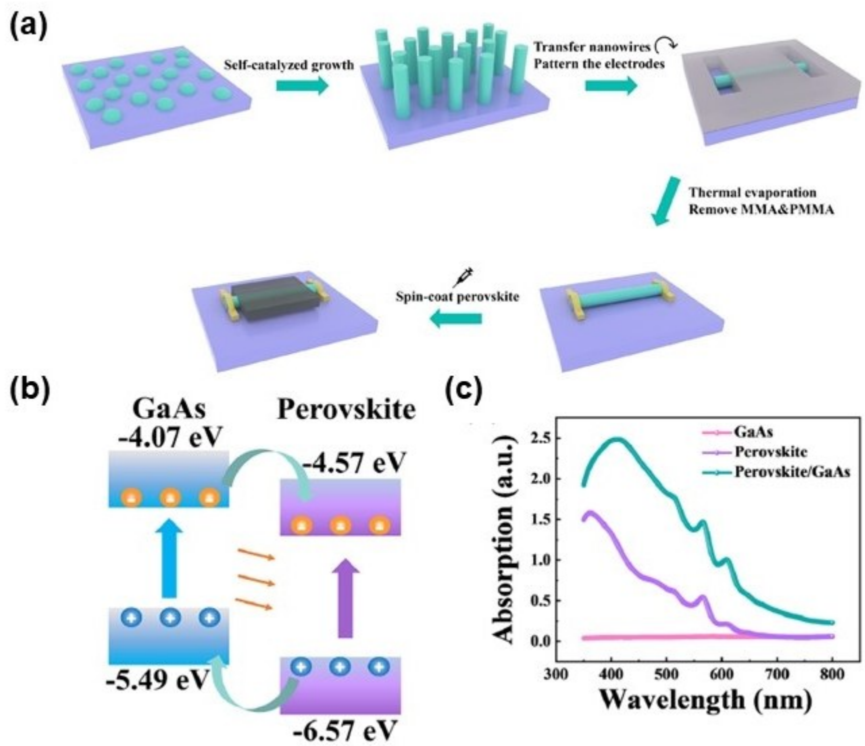

图8 (a)钙钛矿/GaAs NW光电探测器制备过程示意图;(b)钙钛矿/GaAs混合结构的能带图;(c)单个GaAs NW、钙钛矿和钙钛矿/GaAs纳米线复合结构的吸收光谱[100]

Fig. 8 (a) Schematic illustration of the preparation process for a perovskite/GaAs NW photodetector; (b) Energy band diagram of the perovskite/GaAs hybrid structure; (c) Absorption spectra of individual GaAs NW, perovskite, and perovskite/GaAs nanowire composite structure[100]

光电探测器相比,275 nm处$CsPb(BrCl)_3$:Yb^{3+}/Ge的响应速度提高1.21 μs,且1310 nm处的响应度提高80%,这项工作实现光电探测器UV-NIR波段集成[107]。除了Ge,Cong等[108]制备基于$CsPbBr_3$/GeSn异质结的宽带光电探测器。该器件的探测范围可覆盖450-2200 nm。在532 nm波长下,响应度比纯GeSn探测器提高了4.92倍,IR波段的响应度也得到提升。该探测器的响应度比GeSn器件大1.42倍,且该器件显示出良好的稳定性。

4.2.4 钙钛矿/碳材料宽谱带光电探测器

除以上典型的半导体晶体材料,碳材料(如石墨、炭黑、碳纳米管、石墨烯等)由于其具有高导电性、化学稳定性、低成本等优点,在光电探测器等领域广泛应用[109-113]。特别是石墨烯具有卓越的机械性能和极高的载流子迁移率(高达200000 cm^2/Vs)[114, 115]。Lee等[116]制备石墨烯/钙钛矿复合器件,其在Vis区域的响应度高达180 A/W,远高于纯钙钛矿器件的0.49 A/W。另外,Zhou等[114]制备多层结构"石墨烯/PTAA/钙钛矿/PMMA"构成的柔性光电探测器,能够检测UV-NIR响应,且在360 nm处该器件显示出高达10^{13} Jones的探测率和10^5 A/W的响应度。由于PMMA层的保护,该器件具有高弯曲耐用性、快响应时间和良好的空气稳定性。Li等[87]通过钙钛矿/单壁碳纳米管复合光活性层,改善载流子传输并减少载流子复合损耗,制备高灵敏度宽带光电探测器,单层石墨烯与$MAPbI_3$的复合显著增强光响应,其探测率在Vis区域超过3.8×10^{12} Jones,在NIR区域超过1.2×10^{12} Jones,响应速度小于15 μs。石墨烯具有宽吸收带,而甲基铵卤化铅钙钛矿具有高吸收截面,两者的结合提供较高的光电流和超高的外量子效率[117]。Li等[118]还首次提出钙钛矿/石墨烯复合的自供电型光电探测器。由于石墨烯独特的电荷传输特性和钙钛矿的强光吸收特性,该光电探测器具有260-900 nm的宽检测范围、实现4×10^6的超高开关比。

4.3 钙钛矿/量子点、染料、上转换材料宽谱带光电探测器

4.3.1 钙钛矿/染料宽谱带光电探测器

具有NIR吸收的有机染料(如酞菁染料、卟啉类染料)能够与钙钛矿结合,构筑宽谱带光电探测

器[119, 120]。早在 2016 年，Teng 等[121]就通过 Rhodamine B 改性的 $MAPbI_3$ 复合光电探测器，该探测器对 550 nm 显示出 43. 6 mA/W 的高响应度和 286 的高开关比，在 500 μW/cm^2 的功率下对 Vis 有良好的响应。进一步拓宽钙钛矿响应波长，Lin 等[39]制备新型超宽带有机染料-钙钛矿复合光电探测器，具有 NIR 和短波长 IR 响应。图 9b 为 $CyPF_6$/$Cy1BF_4$ 的分子结构，该探测器响应范围能够延伸至 1. 6 μm。Chen 等[122]通过 $MAPbI_3$ 和 PDPP3T 复合（图 9c）不仅实现了 NIR 区灵敏的光响应，而且在 UV-Vis 具有 8. 8×10^{10} Jones 的高光谱响应度，实现了 550-940 nm 区域表现出互补吸收。

4. 3. 2 钙钛矿/QDs 宽谱带光电探测器

PbX（X=S、Te、Se）基 QDs 具有易于制备、低成本加工、优异的空气稳定性和可调节的带隙（0. 40-2. 0 eV），在 825-1750 nm 的宽波段范围有明显优势[123-125]。此外，PbX QDs 由于其较低的激子离解能、优良的载流子迁移率以及较大的吸收截面，使得齐能实现大量的 IR 吸收[126]。Karani 等[123]通过 $MAPbI_3$/PbS QDs 复合（图 9d），即钙钛矿吸收 UV-Vis 的高能光子而 PbS QDs 吸收 NIR 低能光子。如图 9e 所示，通过两个不同 EQE 光谱发现 1100 nm 以上的 IR 光子吸收延长。Song 等[127]利用 $Cu_2CdZn_{1-x}SnS_4$ QDs 可以将 $MAPbI_3$ 响应范围扩大到 900 nm，其中 830 nm 附近的波段明显增加。Zhang 等[128]通过 SCN^- 钝化的 PbS 胶体 QDs 与 $MAPbI_3$ 结合获得 UV-NIR 宽带光电探测器（图 9f），实现了对 365-1550 nm 的宽谱响应。为了提升 Vis 和 NIR 的 EQE，Gong 等[129]利用 $MAPbI_3$ 和 PbS QDs 复合获得超灵敏的宽带光电探测器。$MAPbI_3$ 在 375-1100 nm 的 UV-Vis 区域具有超过 300 mA/W 和 130 mA/W 的高响应度，且探测率分别超过 10^{13} Jones 和 5×10^{12} Jones，得到与原始无机器件相当的器件性能参数。

除了 PbS QDs 外，Si QDs 可以吸收短波长（< 500 nm）区域的光，并在 600 - 900 nm 区域发射光[130, 131]，Ren 等[132]将钙钛矿与胶体 Si QDs 复合，通过在其表面均匀覆盖一层纳米孔隙 PMMA 反射抑制膜，提升 3% 的 Vis 到 NIR 范围的透射率，实现更高的 365、465 和 525 nm 的外量子效率。Subramanian 等[115]制备基于高质量白色荧光石墨烯 QDs 和 $MAPbI_3$ 复合薄膜。与纯 $MAPbI_3$ 相比，在 -3 V 偏压下，得到超过两倍的光暗电流比、12 A/W 的高响应度、6. 5×10^{11} Jones 的探测率，以及更快的响应速度，在 300-600 nm 区域具有很强的光吸收，并将其吸收范围扩展到 NIR 区域（图 9g）。

4. 3. 3 钙钛矿/上转换材料宽谱带光电探测器

上转换材料吸收 NIR 并通过非线性光学过程将其上转换为能量更高的可见光子，其基本过程是通过中间态吸收两个 NIR 光子，从基态跃迁到高能级[133-135]。一般来说，上转换材料由主体材料（如 $NaYF_4$ 和 $NaGdF_4$）和稀土掺杂剂（通常是 Yb^{3+}/Ho^{3+}，Yb^{3+}/Er^{3+} 或 Yb^{3+}/Tm^{3+}）组成[136-138]。光子上转换过程中，其中低能量的光被转换为高能量的光。这一过程通常涉及到多个光子的吸收和一个光子的发射。其过程包括，多光子吸收即材料吸收两个或更多的低能光子。这些光子的能量通常低于材料带隙的能量，因此它们不能单独激发电子跃迁到导带；发射高能光子即处于激发态的电子最终回到基态，过程中释放一个能量高于吸收光子能量之和的光子，实现上转换过程。这个过程中发出的光子具有较短的波长。

Zhang 等[139]将 TiO_2：Er^{3+} 纳米棒阵列作为用于钙钛矿的上转换材料。TiO_2：Er^{3+} 纳米棒在 710-1200 nm 范围内具有较宽的吸收，可通过上转换发射绿光。Zhao 等[140]通过引入一种新型的 $CsPbF_3$:Zn^{2+},Yb^{3+},Tm^{3+} 基钙钛矿上转化纳米晶体，该晶体在 980 nm 的 NIR 区域具有优异的响应性，外量子效率为 135%。另外，Zhang 等[33]通过 $MAPbI_3$ 微阵列与 $NaYF_4$:Yb/Er 上转换纳米粒子集成的柔性平面光电探测器，实现在 Vis 增强的光子吸收、在 NIR 的高效能量转换。该器件具有高达 5. 9×10^{12} Jones 的检测度，且在 980 nm 处获得优异的 NIR 光响应，光谱响应度高达 0. 27 A/W。

Pb 基钙钛矿与上转换材料结合，通过多光子吸收 IR 然后发射 UV 和 Vis。因此，与上转换材料的结合可以有效地使 Pb 基钙钛矿光电探测器获得 IR 响应能力。Liu 等[141]采用覆盖了一层 20-30 nm 厚的 $NaYF_4$:Yb/Er 将钙钛矿的探测波段扩展到 1100 nm。顶层 $NaYF_4$:Yb/Er 可以将 850-1033 nm 波长的强 NIR 吸收转变为 400-670 nm 波长的光发射。Zhang 等[142]通过低温旋涂法制备基于 α-$CsPbI_3$ QDs 和 $NaYF_4$:Yb,Er QDs 的复合光电探测器，其光学响应可扩展到 NIR 区域，具有 1. 5 A/W 的响应度、10^4 的开关比和 5 /5 ms 的上升/衰减时间。

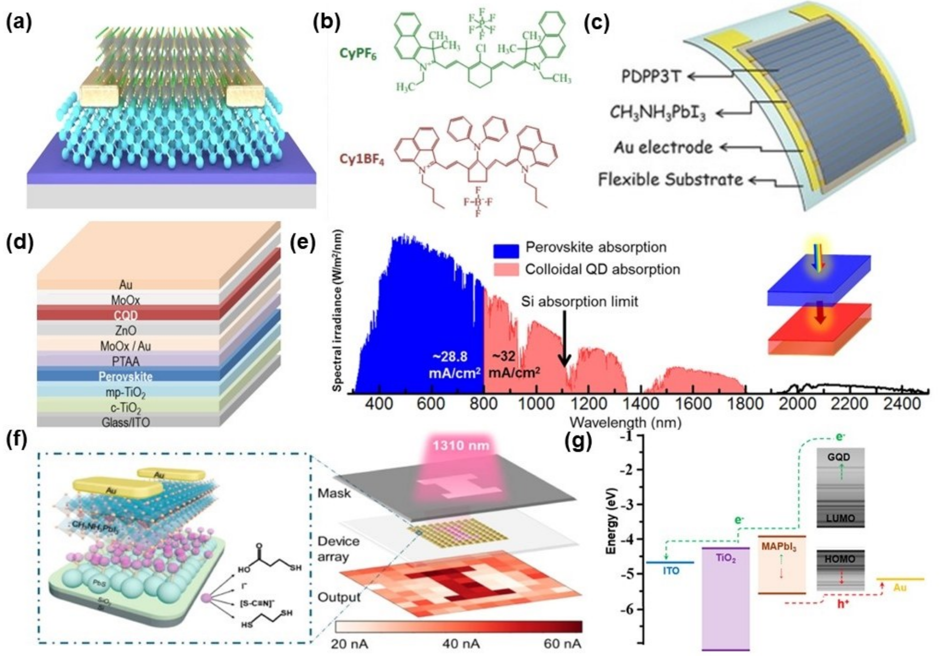

图9(a) 钙钛矿/Ge异质结光电探测器三维示意图[105];(b)$CyPF_6$/$Cy1BF_4$的化学结构图[39];(c) $MAPbI_3$和PDPP3T作为光敏剂的柔性器件结构图[122];(d)钙钛矿/量子点探测器结构图[123];(e)太阳光谱显示了典型钙钛矿太阳能电池在1.55 eV带隙下产生光电流的极限,以及低带隙CQDs可以捕获的低能光子[123];(f)基于$PbS/MAPbI_3$复合材料的宽带光电探测器[128];(g) GQD/$MAPbI_3$器件的能级图和电荷转移机理[115]

Fig. 9 (a) Three-dimensional schematic diagram of heterojunction photodetector[105]; (b) Chemical structure diagram of $CyPF_6$/$Cy1BF_4$[39]; (c) Structural diagram of flexible device with $MAPbI_3$ and PDPP3T as sensitizers[122]; (d) Device structure diagram of ITO/c-TiO_2/mp-TiO_2/Perovskite/PTAA/(MoO_x/Au)/ZnO/CQD/MoO_x/Au[123]; (e) The solar spectrum displays the limit of photocurrent generation at a 1.55 eV bandgap for typical perovskite solar cells, as well as the low-energy photons that can be captured by low-bandgap CQDs[123]; (f) Device structure of a broadband photodetector based on PbS/$MAPbI_3$ composite material and schematic representation of ligands used for exchange[128]; (g) Energy level diagram and charge transfer mechanism of GQD/$MAPbI_3$ device[115]

5 总结和展望

混合卤化物钙钛矿是理想的光电材料,且可以与商业Si和Ge基NIR器件相媲美,但是其IR区域的响应仍受限。目前,Sn-Pb混合或Sn基钙钛矿光电探测器仅能够在1060 nm波长范围内实现高响应率和高检测率,进一步提升其宽谱红外响应仍有限。未来的研究将集中于改善Sn基钙钛矿在光照、湿度、温度变化下的稳定性。开发新型器件结构,如复合异质结、QDs表面修饰钝化、还原剂抑制氧化等,可提高光电探测器的响应速度、灵敏度和信噪比。因此,Sn基钙钛矿光电探测器领域存在广阔的研究空间和巨大的应用潜力。通过不断探索和改进,有望实现高性能、高稳定性的Sn基钙钛矿光电探测器。

与其他半导体材料复合集成是拓宽其响应范围有效方案。将钙钛矿和有机半导体结合可以有效地拓宽光谱的响应范围,制备高灵敏度且响应速度快的钙钛矿有机异质结光电探测器,该探测器可溶液加工且吸收谱带易于化学调控。钙钛矿和Si的复合可提升钙钛矿的光电子集成特性,用于高灵敏度和宽带光探测。但钙钛矿/Si的响应范围被限制在1100 nm,钙钛矿和Ge基半导体相结合是一种较为理想的方案,仍需考虑其存在界面电子传输的问题。通过改变染料分子或添加共轭配体来调节其吸收谱范围,利用染料分子红外吸收的特性实现从UV-Vis-NIR光谱的有效吸收响应。然而,染料分子的稳定性也可能受到光照和氧化等因素的影响导致染料逐渐失效。QDs由于其较低的激子离解能、优良的载流子迁移率和较大的吸收截面,是实现IR互补响应吸收的理想材料。开发新型的量子点,如SnTe,PbSe,PbTe,CuInSe等,是未来需要重点尝试的复合方案。上转换材料吸收NIR并通过非线性光学过程转换为更高能量的可见光,但是上转换的效率比较低,通

常需要高能量的激光来激发。综上，为实现基于钙铁矿的宽谱带IR光电探测器和成像阵列商业化应用，需进一步探索和努力解决光谱扩展、像素集成、灵活性和稳定性等方面的问题。

参 考 文 献：

[1] 苏宛然，冯琳，石林林，等．表面等离激元增强型光电探测器研究进展［J］．发光学报，2021，42(07)：1014-1028.
SU W R, FENG L, SHI L L, *et al*. Progress in research on surface plasmon enhanced photodetectors [J]. *Chin. J. Lumin.*, 2021, 42(07): 1014-1028. (in Chinese)

[2] WEI Y-F, LI G-H, PAN D, *et al*. Research progress towards perovskite electrical driven lasers [J]. *Chin. J. Lumin.*, 2022, 43(10): 1478-1494.

[3] 刘佳男，王芷，闫翎鹏，等．光学增益介质在微型激光器中的应用进展［J］．发光学报，2022，43(12)：1948-1964.
LIU J N, WANG Z, YAN L P, *et al*. Progress in the application of optical gain media in micro-lasers [J]. *Chin. J. Lumin.*, 2022, 43(12): 1948-1964. (in Chinese)

[4] 朱立华，商雪妮，雷凯翔，等．应用于钙钛矿太阳能电池中金属氧化物电子传输材料的研究进展［J］．发光学报，2020，41(05)：481-497
ZHU L H, SHANG X N, LEI K X, *et al*. Research progress on metal oxide electron transport materials applied in perovskite solar cells [J]. *Chin. J. Lumin.*, 2020, 41(05): 481-497. (in Chinese)

[5] 朱云飞，赵雪帆，王成麟，等．赝卤素阴离子工程在钙钛矿太阳能电池中的应用研究进展［J］．发光学报，2023，44(04)：579-597
ZHU Y F, ZHAO X F, WANG C L, *et al*. Progress in research on pseudo-halide anion engineering in perovskite solar cells [J]. *Chin. J. Lumin.*, 2023, 44(04): 579-597. (in Chinese)

[6] ZHANG Y, QIN Z, NIE W, *et al*. High-performance $MAPbI_3$/PM6:Y6 perovskite/organic hybrid photodetectors with a broadband response [J]. *Adv. Opt. Mater.*, 2022, 10(18): 1-8.

[7] 练惠旺，康茹，陈星中，等．全无机钙钛矿$CsPbX_3$热稳定性研究进展［J］．发光学报，2020，41(08)：926-939
LIAN H W, KANG R, CHEN X Z, *et al*. Progress in research on the thermal stability of all-inorganic perovskite $CsPbX_3$ [J]. *Chin. J. Lumin.*, 2020, 41(08): 926-939. (in Chinese)

[8] 魏衍福，李国辉，潘登，等．通向钙钛矿电泵浦激光的研究进展［J］．发光学报，2022，43(10)：1478-1494.
WEI Y F, LI G H, PAN D, *et al*. Research progress towards perovskite electrically pumped lasers [J]. *Chin. J. Lumin.*, 2022, 43(10): 1478-1494. (in Chinese)

[9] HAN J, CHAI Y, LI X. Research progress on structure design of direct halogen perovskite X-ray detectors [J]. *Chin. J. Lumin.*, 2024, 45(1): 25-43.

[10] GEOSPATIAL N. The electromagnetic spectrum [Z]. 2019.

[11] ARORA N, DAR M I, HINDERHOFER A, *et al*. Perovskite solar cells with CuSCN hole extraction layers yield stabilized efficiencies greater than 20 [J]. *Science*, 2017, 358(6364): 768-771.

[12] JOKAR E, CAI L, HAN J, *et al*. Emerging opportunities in lead-free and lead–tin perovskites for environmentally viable photodetector applications [J]. *Chem. Mater.*, 2023, 35(9): 3404-3426.

[13] WALSH A, SCANLON D O, CHEN S, *et al*. Self-regulation mechanism for charged point defects in hybrid halide perovskites [J]. *Angew. Chem.*, *Int. Ed.*, 2015, 127(6): 1811-1814.

[14] QIANQIAN, ARMIN, ARDALAN, *et al*. Filterless narrowband visible photodetectors [J]. *Nature photonics*, 9: 687-694.

[15] DU J S, SHIN D, STANEV T K, *et al*. Halide perovskite nanocrystal arrays: Multiplexed synthesis and size-dependent emission [J]. *Science Advances*, 2020, 6(39): 4959.

[16] YAN J-H, CHEN S-X, YANG J-B, *et al*. Improving efficiency and stability of organic-inorganic hybrid perovskite solar cells by absorption layer ion doping [J]. *Acta Physica Sinica*, 2021, 70(20): 206801-206810.

[17] SHI D, ADINOLFI V, COMIN R, *et al*. Low trap-state density and long carrier diffusion in organolead trihalide perovskite single crystals [J]. *Science*, 2015, (347-Jan. 30 TN. 6221).

[18] 杨敏，岳鹏，廉岚淇，等．基于声化学法合成的$CsPbBr_3$钙钛矿微晶双光子发光特性［J］．发光学报，2022，43(8)：1207-1216.

YANG M, YUE P, LIAN L Q, *et al.* Two-photon luminescence characteristics of CsPbBr3 perovskite microcrystals synthesized by sonochemical method [J]. *Chin. J. Lumin.*, 2022, 43(8): 1207-1216. (in Chinese)

[19] FANG Y, DONG Q, SHAO Y, *et al.* Highly narrowband perovskite single-crystal photodetectors enabled by surface-charge recombination [J]. *Nature Photonics*, 2015, 9(10): 679-686.

[20] HU X, ZHANG X, LIANG L, *et al.* High-performance flexible broadband photodetector based on organolead halide perovskite [J]. *Adv. Funct. Mater.*, 2014, 24(46): 7373-7380.

[21] XIAO L, XU J, LUAN J, *et al.* Preparation of $CH_3NH_3PbCl_3$ film with a large grain size using PbI_2 as Pb source and its application in photodetector [J]. *Materials Letters*, 2018, 220: 108-111.

[22] 赵雪帆, 朱云飞, 孟凡斌, 等. 非铅钙钛矿光伏材料与器件研究进展[J]. 发光学报, 2022, 43(06): 817-832
ZHAO X F, ZHU Y F, MENG F B, *et al.* Progress in research on lead-free perovskite photovoltaic materials and devices [J]. *Chin. J. Lumin.*, 2022, 43(06): 817-832. (in Chinese)

[23] LI M, LI F, GONG J, *et al.* Advances in Tin(II)-based perovskite solar cells: from material physics to device performance [J]. *Small Structures*, 2022, 3(1): 2100102.

[24] JIANG X, LI H, ZHOU Q, *et al.* One-step synthesis of $SnI_2(DMSO)_x$ adducts for high-performance Tin perovskite solar cells [J]. *J. Am. Chem. Soc.*, 2021, 143(29): 10970-10976.

[25] YU B B, CHEN Z, ZHU Y, *et al.* Heterogeneous 2D/3D tin-halides perovskite solar cells with certified conversion efficiency breaking 14% [J]. *Adv Mater*, 2021, 33(36): 2102055.

[26] CAO J, YAN F. Recent progress in tin-based perovskite solar cells [J]. *Energy & Environmental Science*, 2021, 14(3): 1286-1325.

[27] LIN R, XIAO K, QIN Z, *et al.* Monolithic all-perovskite tandem solar cells with 24.8% efficiency exploiting comproportionation to suppress Sn(ii) oxidation in precursor ink [J]. *Nature Energy*, 2019, 4(10): 864-873.

[28] TSAREV S, BOLDYREVA A G, LUCHKIN S Y, *et al.* Hydrazinium-assisted stabilisation of methylammonium tin iodide for lead-free perovskite solar cells [J]. *J. Mater. Chem. A*, 2018, 6(43): 21389-21395.

[29] BABAYIGIT A, THANH DDUY, ETHIRAJAN A, *et al.* Assessing the toxicity of Pb- and Sn-based perovskite solar cells in model organism Danio rerio [J]. *Nature*, 2016, 6: 18721.

[30] TAI Q, GUO X, TANG G, *et al.* Antioxidant grain passivation for air-stable Tin-based perovskite solar cells [J]. *Angew. Chem., Int. Ed.*, 2019, 58(3): 806-810.

[31] LIU C K, TAI Q, WANG N, *et al.* Sn-based perovskite for highly sensitive photodetectors [J]. *Adv Sci* 2019, 6(17): 1900751.

[32] LIU C-K, TAI Q, WANG N, *et al.* Lead-free perovskite/organic semiconductor vertical heterojunction for highly sensitive photodetectors [J]. *ACS Appl. Mater. Interfaces*, 2020, 12(16): 18769-18776.

[33] ZHANG H, XIAO Y, QI F, *et al.* Near-infrared light-sensitive hole-transport-layer free perovskite solar cells and photodetectors with hexagonal $NaYF_4$: Yb^{3+}, Tm^{3+}@SiO_2 upconversion nanoprism-modified TiO_2 scaffold [J]. *ACS Sustainable Chem. Eng.*, 2019, 7(9): 8236-8244.

[34] STOUMPOS C C, MALLIAKAS C D, KANATZIDIS M G. Semiconducting tin and lead iodide perovskites with organic cations: phase transitions, high mobilities, and near-infrared photoluminescent properties [J]. *Inorg. Chem.*, 2013, 52(15): 9019-9038.

[35] CAO F, TIAN W, WANG M, *et al.* Stability enhancement of lead-free $CsSnI_3$ perovskite photodetector with reductive ascorbic acid additive [J]. *InfoMat*, 2020, 2(3): 577-584.

[36] SHAO D, ZHU W, XIN G, *et al.* A high performance UV – visible dual-band photodetector based on an inorganic Cs_2SnI_6 perovskite/ZnO heterojunction structure [J]. *J. Mater. Chem. C*, 2020, 8(5): 1819-1825.

[37] KRISHNAIAH M, KIM S, KUMAR A, *et al.* Physically detachable and operationally stable Cs_2SnI_6 photodetector arrays integrated with μ-LEDs for broadband flexible optical systems [J]. *Adv. Mater.*, 2022, 34(17): 2109673.

[38] ZHU H, LIU A, ZOU T, *et al.* A Lewis base and boundary passivation bifunctional additive for high performance lead-free layered-perovskite transistors and phototransistors [J]. *Mater. Today Energy*, 2021, 21: 100722.

[39] LIN Q, WANG Z, YOUNG M, *et al.* Near-infrared and short-wavelength infrared photodiodes based on dye – perovskite composites [J]. *Adv. Funct. Mater.*, 2017, 27(38): 1702485.

[40] ZHU H L, CHOY W C H J S R. Crystallization, properties, and challenges of low-bandgap Sn-Pb binary perovskites

[J]. *Solar RRL*, 2018, 2(10).

[41] KORSHUNOVA K, WINTERFELD L, BEENKEN W J D, *et al*. Thermodynamic stability of mixed Pb:Sn methyl-ammonium halide perovskites [J]. *physica status solidi*, 2016, 253(10): 1907-1915.

[42] CHEN Z, LIU M, LI Z, *et al*. Stable Sn/Pb-based perovskite solar cells with a coherent 2D/3D interface [J]. *iScience*, 2018, 9: 337-346.

[43] MAHATA A, MEGGIOLARO D, DE ANGELIS F. From ;arge to small polarons in lead, Tin, and mixed lead-Tin halide perovskites [J]. *J. Phys. Chem. Lett.*, 2019, 10(8): 1790-1798.

[44] WANG W, ZHAO D, ZHANG F, *et al*. Highly sensitive low-bandgap perovskite photodetectors with response from Ultraviolet to the Near-Infrared Region [J]. *Adv. Funct. Mater.*, 2017, 27(42): 1703953.

[45] XU X, C-CCHUEH, YANG Z, *et al*. Ascorbic acid as an effective antioxidant additive to enhance the efficiency and stability of Pb/Sn-based binary perovskite solar cells [J]. *Nano Energy*, 2017, 34: 392-398.

[46] ZHAO Y, LI C, JIANG J, *et al*. Sensitive and stable Tin–lead hybrid perovskite photodetectors enabled by double-sided surface passivation for infrared upconversion detection [J]. *Small*, 2020, 16(26).

[47] LI W, CHEN J, LIN H, *et al*. The UV–VIS-NIR broadband ultrafast flexible Sn-Pb perovskite photodetector for multispectral imaging to distinguish substance and foreign-body in biological tissues [J]. *Adv. Opt. Mater.*, 2024, 12(2): 2301373.

[48] CHANG Z, LU Z, DENG W, *et al*. Narrow-bandgap Sn–Pb mixed perovskite single crystals for high-performance near-infrared photodetectors [J]. *Nanoscale*, 2023, 15(10): 5053-5062.

[49] CHANG C-Y, WU K-H, CHANG C-Y, *et al*. Enhanced performance and stability of low-bandgap mixed lead–tin halide perovskite photovoltaic solar cells and photodetectors via defect passivation with UiO-66-NH_2 metal–organic frameworks and interfacial engineering [J]. *Mol. Syst. Des. Eng.*, 2022, 7(9): 1073-1084.

[50] KIM H, KIM R M, NAMGUNG S D, *et al*. Ultrasensitive near-infrared circularly polarized light detection using 3D perovskite embedded with chiral plasmonic nanoparticles [J]. *Adv Sci* 2022, 9(5): e2104598.

[51] LIU H, ZHU L, ZHANG H, *et al*. Realizing high-detectivity near-infrared photodetectors in tin–lead perovskites by double-sided surface-preferred distribution of multifunctional tin thiocyanate additive [J]. *ACS Energy Letters*, 2023, 8(1): 577-589.

[52] 韩鹏，刘鹤，国凤云，等. BiI_3修饰$Cs_3Bi_2I_9$自供能光电化学型探测器制备及其性能 [J]. 发光学报，2023, 44(08): 1471-1478

HAN P, LIU H, GUO F Y, *et al*. Fabrication and properties of a self-powered photoelectrochemical detector based on BiI_3-modified $Cs_3Bi_2I_9$ [J]. *Chin. J. Lumin.*, 2023, 44(08): 1471-1478. (in Chinese)

[53] XIE C, YAN F. Flexible photodetectors based on novel functional materials [J]. *Small Methods*, 2017, Vol. 13 (No. 43): 1701822.

[54] 卢璐，董建华，池淑瑞，等. 基于山梨醇钝化的绿光多晶薄膜钙钛矿发光二极管 [J]. 发光学报，2023, 44(10): 1833-1841.

LU L, DONG J H, CHI S R, *et al*. Green light polycrystalline thin film perovskite light-emitting diodes based on sorbitol passivation [J]. *Chin. J. Lumin.*, 2023, 44(10): 1833-1841. (in Chinese)

[55] 董建华，卢璐，金旭东，等. 葡萄糖作钝化剂的绿光多晶薄膜钙钛矿发光二极管 [J]. 发光学报，2023, 44(2): 328-336.

DONG J H, LU L, JIN X D, *et al*. Green light polycrystalline thin film perovskite light-emitting diodes with glucose as a passivating agent [J]. *Chin. J. Lumin.*, 2023, 44(2): 328-336. (in Chinese)

[56] ZHAO X, ZHANG Z, ZHU Y, *et al*. Rationally tailoring chiral molecules to minimize interfacial energy loss enables efficient and stable perovskite solar cells using vacuum flash technology [J]. *Nano Lett*, 2023, 23(23): 11184-11192.

[57] FU Q, WANG X, LIU F, *et al*. Ultrathin ruddlesden-popper perovskite heterojunction for sensitive photodetection [J]. *Small*, 2019, 15(39): e1902890.

[58] GUO Z, ZHANG J, LIU X, *et al*. Optoelectronic synapses and photodetectors based on organic semiconductor/halide perovskite heterojunctions: materials, devices, and applications [J]. *Adv. Funct. Mater.*, 2023, 33(46): 2305508.

[59] CAO F, TIAN W, DENG K, *et al*. Self-powered UV–Vis–NIR photodetector based on conjugated-polymer/$CsPbBr_3$ nanowire Array [J]. *Adv. Funct. Mater.*, 2019, 29(48): 1906756.

[60] CHEN S, TENG C, ZHANG M, *et al*. A flexible UV - Vis - NIR photodetector based on a perovskite/conjugated-polymer composite [J]. *Adv. Mater.*, 2016, 28(28): 5969-5974.

[61] LI C, WANG H, WANG F, *et al*. Ultrafast and broadband photodetectors based on a perovskite/organic bulk heterojunction for large-dynamic-range imaging [J]. *Light: Sci. Appl.*, 2020, 9(1): 31.

[62] XIE C, YOU P, LIU Z, *et al*. Ultrasensitive broadband phototransistors based on perovskite/organic-semiconductor vertical heterojunctions [J]. *Light: Sci. Appl.*, 2017, 6(8): e17023-e17023.

[63] LIANG SHEN, YUZE LIN, CHUNXIONG BAO, *et al*. Integration of perovskite and polymer photoactive layers to produce ultrafast response, ultraviolet-to-near-infrared, *sensitive photodetectors; proceedings of the The fifth symposium on new solar cells*, [F].

[64] WU G, FU R, CHEN J, *et al*. Perovskite/organic bulk-heterojunction integrated ultrasensitive broadband photodetectors with high Near-Infrared external quantum efficiency over 70% [J]. *Small*, 2018, 14(39): 1802349.

[65] YUAN J, ZHANG Y, ZHOU L, *et al*. Single-junction organic solar cell with over 15% efficiency using fused-ring acceptor with electron-deficient core [J]. *JOULE*, 2019, 3(4): 1140-1151.

[66] ZHANG Y, QIN Z, NIE W, *et al*. High-performance $MAPbI_3/PM_6$:Y6 perovskite/organic hybrid photodetectors with a broadband response [J]. *Adv. Opt. Mater.*, 2022, 10(18): 2200648.

[67] GAO Y, XU W, ZHANG S-W, *et al*. Double cascading charge transfer at integrated perovskite/organic bulk heterojunctions for extended Near-Infrared photoresponse and enhanced photocurrent [J]. *Small*, 2022, 18(12): 2106083.

[68] ZHANG Y, QIN Z, HUO X, *et al*. High-performance near-infrared photodetectors based on the synergy effect of short wavelength light filter and long wavelength response of a perovskite/polymer hybrid structure [J]. *ACS Appl. Mater. Interfaces*, 2021, 13(51): 61818-61826.

[69] CHEN K, ZHANG X, CHEN P-A, *et al*. Solution-processed $CsPbBr_3$ quantum dots/oorganic semiconductor planar heterojunctions for high-performance photodetectors [J]. *Adv. Sci.*, 2022, 9(12): 2105856.

[70] TYZNIK C, LEE J, SORLI J, *et al*. Photocurrent in metal-halide perovskite/organic semiconductor heterostructures: impact of microstructure on charge generation efficiency [J]. *ACS Appl. Mater. Interfaces*, 2021, 13(8): 10231-10238.

[71] LI X, XIANG Y, WAN J, *et al*. Three-dimensional pyramidal $CsPbBr_3$/C8BTBT film heterojunction photodetectors with high responsivity and long-term stability [J]. *Org. Electron.*, 2022, 101: 106409.

[72] TONG S, SUN J, WANG C, *et al*. High-performance broadband perovskite photodetectors based on $CH_3NH_3PbI_3$/C8BTBT heterojunction [J]. *Adv. Electron. Mater.*, 2017, 3(7): 1700058.

[73] LIN Q, ARMIN A, LYONS D M, *et al*. Low noise, IR-blind organohalide perovskite photodiodes for visible light detection and imaging [J]. *Adv. Mater.*, 2015, 27(12): 2060-2064.

[74] TANG F, CHEN Q, CHEN L, *et al*. Mixture interlayer for high performance organic-inorganic perovskite photodetectors [J]. *Appl. Phys. Lett.*, 2016, 109(12).

[75] LIU T, JIA Z, SONG Y, *et al*. Near infrared self-powered organic photodetectors with a record responsivity enabled by low trap density [J]. *Adv. Funct. Mater.*, 2023, 33(25): 2301167.

[76] ZHANG Q, ZHANG M, ZHANG F, *et al*. Understanding the mechanisms of a conjugated polymer electrolyte for interfacial modification in solution-processed organic-inorganic hybrid perovskite photodetectors [J]. *Org. Electron.*, 2020, 83: 105729.

[77] BAO C, ZHU W, YANG J, *et al*. Highly flexible self-powered organolead trihalide perovskite photodetectors with gold nanowire networks as transparent electrodes [J]. *ACS Appl. Mater. Interfaces*, 2016, 8(36): 23868-23875.

[78] ZHU H L, LIN H, SONG Z, *et al*. Achieving high-quality Sn - Pb perovskite films on complementary metal-oxide-semiconductor-compatible metal/silicon substrates for efficient imaging array [J]. *ACS Nano*, 2019, 13(10): 11800-11808.

[79] LI L, CHEN H, FANG Z, *et al*. An electrically modulated single-color/dual-color imaging photodetector [J]. *Adv. Mater.*, 2020, 32(24): 1907257.

[80] CHANG C-Y, WU K-S, CHANG C-Y. N-type conjugated polymer as multi-functional interfacial layer for high-performance and ultra-stable self-powered photodetectors based on perovskite nanowires [J]. *Adv. Funct. Mater.*, 2022, 32(8): 2108356.

[81] MA N, JIANG J, ZHAO Y, *et al*. Stable and sensitive tin-lead perovskite photodetectors enabled by azobenzene derivative for near-infrared acousto-optic conversion communications [J]. *Nano Energy*, 2021, 86: 106113.

[82] XIA H, TONG S, ZHANG C, *et al*. Flexible and air-stable perovskite network photodetectors based on $CH_3NH_3PbI_3$/C8BTBT bulk heterojunction [J]. *Appl. Phys. Lett.*, 2018, 112(23).

[83] ZOU C, XI Y, HUANG C-Y, *et al*. A highly densitive UV - vis - NIR all-Inorganic perovskite quantum dot phototransistor based on a layered heterojunction [J]. *Adv. Opt. Mater.*, 2018, 6(14): 1800324.

[84] XIE C, YAN F. Perovskite/Poly(3-hexylthiophene)/Graphene multiheterojunction phototransistors with ultrahigh gain in broadband wavelength region [J]. *ACS Appl. Mater. Interfaces*, 2017, 9(2): 1569-1576.

[85] XU X, DENG W, ZHANG X, *et al*. Dual-band, high-performance phototransistors from hybrid perovskite and organic crystal array for secure communication applications [J]. *ACS Nano*, *2019*, 13(5): 5910-5919.

[86] LUO L-B, WU G-A, GAO Y, *et al*. A highly sensitive perovskite/organic semiconductor heterojunction phototransistor and its device optimization utilizing the selective electron trapping effect [J]. *Adv. Opt. Mater.*, 2019, 7(13): 1900272.

[87] LI F, QIU Z, LIU S, *et al*. Carbon nanotube-perovskite composites for ultrasensitive broadband photodiodes [J]. *ACS Appl. Nano Mater.*, 2019, 2(8): 4974-4982.

[88] XU W, GUO Y, ZHANG X, *et al*. Room-temperature-operated ultrasensitive broadband photodetectors by perovskite incorporated with conjugated polymer and single-wall carbon nanotubes [J]. *Adv. Funct. Mater.*, 2018, 28(7): 1705541.

[89] ZHU T, YANG Y, ZHENG L, *et al*. Solution-processed flexible broadband photodetectors with solution-processed transparent polymeric electrode [J]. *Adv. Funct. Mater.*, 2020, 30(15): 1909487.

[90] P-KKUNG, LI M-H, LIN P-Y, *et al*. A review of inorganic hole transport materials for perovskite solar cells [J]. *Advanced Materials Interfaces*, 2018, 5(22): 1800882.

[91] WANG H. High gain single GaAs nanowire photodetector [J]. *Appl. Phys. Lett.*, 2013, 103(9): 093101.

[92] YAO M, HUANG N, CONG S, *et al*. GaAs nanowire array solar cells with axial p - i - n junctions [J]. *Nano Letters*, 2014, 14(6): 3293-3303.

[93] HAN N, YANG Z-X, WANG F, *et al*. High-performance GaAs nanowire solar cells for flexible and transparent photovoltaics [J]. *ACS Appl. Mater. Interfaces*, 2015, 7(36): 20454-20459.

[94] DAI X, ZHANG S, WANG Z, *et al*. GaAs/AlGaAs nanowire photodetector [J]. *Nano Letters*, 2014, 14(5): 2688-2693.

[95] FARRELL A C, MENG X, REN D, *et al*. InGaAs - GaAs nanowire avalanche photodiodes toward single-photon detection in free-running mode [J]. *Nano Letters*, 2019, 19(1): 582-590.

[96] LYSOV A, VINAJI S, OFFER M, *et al*. Spatially resolved photoelectric performance of axial GaAs nanowire pn-diodes [J]. *Nano Research*, 2011, 4(10): 987-995.

[97] LI G, GAO R, HAN Y, *et al*. High detectivity photodetectors based on perovskite nanowires with suppressed surface defects [J]. *Photonics Res.*, 2020, 8(12): 1862-1874.

[98] XIE L, CHEN B, ZHANG F, *et al*. Highly luminescent and stable lead-free cesium copper halide perovskite powders for UV-pumped phosphor-converted light-emitting diodes [J]. *Photonics Res.*, 2020, 8(6): 768-775.

[99] ZHAO Y, LI C, JIANG J, *et al*. Sensitive and stable Tin - lead hybrid perovskite photodetectors enabled by double-sided surface passivation for infrared upconversion detection [J]. *Small*, 2020, 16(26): 2001534.

[100] HOU X, HONG X, LIN F, *et al*. Perovskite/GaAs-nanowire hybrid structure photodetectors with ultrafast multiband response enhancement by band engineering [J]. *Photonics Res.*, 2023, 11(4): 541-548.

[101] ZHANG Z, XU C, ZHU C, *et al*. Fabrication of $MAPbI_3$ perovskite/Si heterojunction photodetector arrays for image sensing application [J]. *Sens. Actuators*, A, 2021, 332: 113176.

[102] GENG X, WANG F, TIAN H, *et al*. Ultrafast photodetector by integrating perovskite directly on silicon wafer [J]. *ACS Nano*, 2020, 14(3): 2860-2868.

[103] LIU J-Q, GAO Y, WU G-A, *et al*. Silicon/perovskite core - shell heterojunctions with light-trapping effect for sensitive self-driven near-infrared photodetectors [J]. *ACS Appl. Mater. Interfaces*, 2018, 10(33): 27850-27857.

[104] CAO F, MENG L, WANG M, *et al*. Gradient energy band driven high-performance self-powered perovskite/CdS photodetector [J]. *Adv Mater*, 2019, 31(12): 1806725.

[105] HU W, CONG H, HUANG W, *et al*. Germanium/perovskite heterostructure for high-performance and broadband photodetector from visible to infrared telecommunication band [J]. *Light: Sci. Appl.*, 2019, 8(1): 106.

[106]YANG Y, LIU X, LIU T, *et al*. High-speed broadband hybrid perovskite nanocrystals /Ge photodetector from UV to NIR [J]. *Adv. Opt. Mater.*, 2023, 11(21): 2300708.

[107]何嘉玉, 陈克强, 冀婷, 等. 基于二维材料的快速响应金属-半导体-金属结构光电探测器研究进展[J]. 发光学报, 2022, 43(05): 745-762

HE J Y, CHEN K Q, JI T, *et al*. Research progress on fast-response metal-semiconductor-metal photodetectors based on two-dimensional materials [J]. *Chin. J. Lumin.*, 2022, 43(05): 745-762. (in Chinese)

[108]CONG H, CHU X, WAN F, *et al*. Broadband photodetector based on inorganic perovskite $CsPbBr_3$/GeSn heterojunction [J]. *Small Methods*, 2021, 5(8): 2100517.

[109]YAVARI M, MAZLOUM-ARDAKANI M, GHOLIPOUR S, *et al*. Carbon nanoparticles in high-performance perovskite solar cells [J]. *Adv. Energy Mater.*, 2018, 8(12): 1702719.

[110]FU X, XU L, LI J, *et al*. Flexible solar cells based on carbon nanomaterials [J]. *Carbon*, 2018, 139: 1063-1073.

[111]XIA C, ZHU S, FENG T, *et al*. Evolution and synthesis of carbon dots: from carbon dots to carbonized polymer dots [J]. *Adv. Sci.*, 2019, 6(23): 1901316.

[112]EBRAHIMI M, KERMANPUR A, ATAPOUR M, *et al*. Performance enhancement of mesoscopic perovskite solar cells with GQDs-doped TiO_2 electron transport layer [J]. *Sol. Energy Mater. Sol. Cells*, 2020, 208: 110407.

[113]LITVIN A P, ZHANG X, USHAKOVA E V, *et al*. Carbon nanoparticles as versatile auxiliary components of perovskite-based optoelectronic devices [J]. *Adv. Funct. Mater.*, 2021, 31(18): 2010768.

[114]ZHOU G, SUN R, XIAO Y, *et al*. A high-performance flexible broadband photodetector based on graphene–PTAA–perovskite heterojunctions [J]. *Adv. Electron. Mater.*, 2021, 7(3): 2000522.

[115]SUBRAMANIAN A, AKRAM J, HUSSAIN S, *et al*. High-performance photodetector based on a graphene quantum dot/ $CH_3NH_3PbI_3$ perovskite hybrid [J]. *ACS Applied Electronic Materials*, 2020, 2(1): 230-237.

[116]LEE Y, KWON J, HWANG E, *et al*. High-performance perovskite–graphene hybrid photodetector [J]. *Adv. Mater.*, 2015, 27(1): 41-46.

[117]LEE Y, KWON J, HWANG E, *et al*. High-performance perovskite–graphene hybrid photodetector [J]. *Adv Mater*, 2015, 27(1): 41-46.

[118]LI J, YUAN S, TANG G, *et al*. High-performance, self-powered photodetectors based on perovskite and graphene [J]. *ACS Appl. Mater. Interfaces*, 2017, 9(49): 42779-42787.

[119]冯印素, 耿涛然, 陈春雷, 等. 半透明钙钛矿太阳能电池的技术关键[J]. 发光学报, 2023, 44(09): 1650-1666

FENG Y S, GENG T R, CHEN C L, *et al*. Key technologies of semi-transparent perovskite solar cells [J]. *Chin. J. Lumin.*, 2023, 44(09): 1650-1666. (in Chinese)

[120]杨立群, 马晓辉, 郑士建, 等. 柔性钙钛矿太阳能电池中电极材料和电荷传输材料的研究进展[J]. 发光学报, 2020, 41(10): 1175-1194.

YANG L Q, MA X H, ZHENG S J, *et al*. Progress in research on electrode materials and charge transport materials in flexible perovskite solar cells [J]. *Chin. J. Lumin.*, 2020, 41(10): 1175-1194. (in Chinese)

[121]TENG C-J, XIE D, SUN M-X, *et al*. Organic dye-sensitized $CH_3NH_3PbI_3$ hybrid flexible photodetector with bulk heterojunction architectures [J]. *ACS Appl. Mater. Interfaces*, 2016, 8(45): 31289-31294.

[122]CHEN S, TENG C, ZHANG M, *et al*. A flexible UV–Vis–NIR photodetector based on a perovskite/conjugated-polymer composite [J]. *Adv Mater*, 2016, 28(28): 5969-5974.

[123]KARANI A, YANG L, BAI S, *et al*. Perovskite/colloidal quantum dot tandem solar cells: Theoretical modeling and monolithic structure [J]. *ACS Energy Letters*, 2018, 3(4): 869-874.

[124]WISE F W. Lead salt quantum dots: the limit of strong quantum confinement [J]. *Acc. Chem. Res.*, 2000, 33(11): 773-780.

[125]皮慧慧, 李国辉, 周博林, 等. 高效率钙钛矿量子点发光二极管研究进展[J]. 发光学报, 2021, 42(05): 650-667

PI H H, LI G H, ZHOU B L, *et al*. Research progress on high-efficiency perovskite quantum dot light-emitting diodes [J]. *Chin. J. Lumin.*, 2021, 42(05): 650-667. (in Chinese)

[126]CHOI J J, WENGER W N, HOFFMAN R S, *et al*. Solution-processed nanocrystal quantum dot tandem solar cells [J]. *Adv Mater*, 2011, 23(28): 3144-3148.

[127]WU Y, BI W, SHI Z, *et al*. Unraveling the dual-functional mechanism of light absorption and hole transport of

$Cu_2Cd_xZn_{1-x}SnS_4$ for achieving efficient and stable perovskite solar cells [J]. *ACS Appl. Mater. Interfaces*, 2020, 12(15): 17509-17518.

[128] ZHANG J-Y, XU J-L, CHEN T, *et al*. Toward broadband imaging: surface-engineered PbS quantum dot/perovskite composite integrated ultrasensitive photodetectors [J]. *ACS Appl. Mater. Interfaces*, 2019, 11(47): 44430-44437.

[129] LIU C, WANG K, DU P, *et al*. Ultrasensitive solution-processed broad-band photodetectors using $CH_3NH_3PbI_3$ perovskite hybrids and PbS quantum dots as light harvesters [J]. *Nanoscale*, 2015, 7(39): 16460-16469.

[130] CHO E-C, PARK S, HAO X, *et al*. Silicon quantum dot/crystalline silicon solar cells [J]. *Nanotechnology*, 2008, 19(24): 245201.

[131] LIU C-Y, HOLMAN Z C, KORTSHAGEN U R. Hybrid solar cells from P3HT and silicon nanocrystals [J]. *Nano letters*, 2009, 9(1): 449-452.

[132] REN S, SHOU C, JIN S, *et al*. Silicon quantum dot luminescent solar concentrators and downshifters with antireflection coatings for enhancing perovskite solar cell performance [J]. *ACS Photonics*, 2021, 8(8): 2392-2399.

[133] KHARE A. A critical review on the efficiency improvement of upconversion assisted solar cells [J]. *J. Alloys Compd.*, 2020, 821: 153214.

[134] HILL S P, DILBECK T, BADUELL E, *et al*. Integrated photon upconversion solar cell via molecular self-assembled bilayers [J]. *ACS Energy Letters*, *2016*, 1(1): 3-8.

[135] 李雅珍，王喜龙，田跃，等. 多光子成像用上转换纳米粒子的单颗粒研究与应用进展 [J]. 发光学报, 2023, 44(11): 2041-2056.

LI Y Z, WANG X L, TIAN Y, *et al*. Progress in single-particle studies and applications of upconversion nanoparticles for multiphoton imaging [J]. *Chin. J. Lumin.*, 2023, 44(11): 2041-2056. (in Chinese)

[136] WANG H Q, BATENTSCHUK M, OSVET A, *et al*. Rare-earth ion doped up-conversion materials for photovoltaic applications [J]. *Adv Mater*, 2011, 23(22-23): 2675-2680.

[137] LIANG L, LIU Y, ZHAO X-Z. Double-shell β-$NaYF_4$:Yb^{3+}, Er^{3+}/SiO_2/TiO_2 submicroplates as a scattering and upconverting layer for efficient dye-sensitized solar cells [J]. *Chem. Commun.*, 2013, 49(38): 3958-3960.

[138] ROH J, YU H, JANG J. Hexagonal β-$NaYF_4$:Yb^{3+}, Er^{3+} nanoprism-incorporated upconverting layer in perovskite solar cells for near-infrared sunlight harvesting [J]. *ACS Appl. Mater. Interfaces*, 2016, 8(31): 19847-19852.

[139] ZHANG H, ZHANG Q, LV Y, *et al*. Upconversion Er-doped TiO_2 nanorod arrays for perovskite solar cells and the performance improvement [J]. *Mater. Res. Bull.*, 2018, 106: 346-352.

[140] DING N, XU W, ZHOU D, *et al*. Upconversion ladder enabled super-sensitive narrowband near-infrared photodetectors based on rare earth doped florine perovskite nanocrystals [J]. *Nano Energy*, 2020, 76: 105103.

[141] LI J, SHEN Y, LIU Y, *et al*. Stable high-performance flexible photodetector based on upconversion nanoparticles/perovskite microarrays composite [J]. *ACS Appl. Mater. Interfaces*, 2017, 9(22): 19176-19183.

[142] ZHANG X, WANG Q, JIN Z, *et al*. Stable ultra-fast broad-bandwidth photodetectors based on α-$CsPbI_3$ perovskite and NaYF4:Yb,Er quantum dots [J]. *Nanoscale*, 2017, 9(19): 6278-6285.

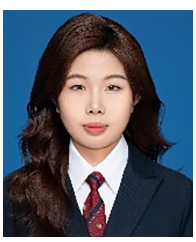

卢孟涵(2001-)，女，天津市人，在读研究生，2023年于天津科技大学获得学士学位，主要从事钙钛矿太阳能电池中光吸收层中缺陷的界面修饰调控策略研究。

E-mail：15122211356@163.com

陈聪(1990—)，男，吉林长春人，博士，河北工业大学 教授，2019年于吉林大学获得博士学位，主要从事面向应用的高效与稳定的光伏电池。E-mail：chencong@hebut.edu.cn

宋宏伟(1967—)，男，黑龙江阿城人，博士，吉林大学 教授，博士生导师，1996年于中国科学院长春物理研究所获得博士学位，主要从事稀土发光材料物理、光电子及生物应用的研究。

E-mail：songhw@jlu.edu.cn